Electrochimica Acta 381 (2021) 138236

Contents lists available at ScienceDirect

Electrochimica Acta

journal homepage: www.elsevier.com/locate/electacta

Insights in electrosynthesis, target binding, and stability of peptide-imprinted polymer nanofilms

Giorgio Caserta[a,*], Xiaorong Zhang[b], Aysu Yarman[b], Eszter Supala[c], Ulla Wollenberger[b], Róbert E. Gyurcsányi[c,*], Ingo Zebger[a,*], Frieder W. Scheller[b,*]

[a] Institut für Chemie, PC 14 Technische Universität Berlin, Straße des 17. Juni 135, 10623 Berlin, Germany
[b] Institute of Biochemistry and Biology, University of Potsdam, Karl-Liebknecht Str. 24-25, 14476 Potsdam, Germany
[c] BME "Lendület" Chemical Nanosensors Research Group, Department of Inorganic and Analytical Chemistry, Budapest University of Technology and Economics, Szt. Gellért tér 4, H-1111 Budapest, Hungary

ARTICLE INFO

Article history:
Received 31 December 2020
Revised 25 February 2021
Accepted 20 March 2021
Available online 30 March 2021

Keywords:
SEIRA spectroelectrochemistry
Peptide imprinting
Electrosynthesis
MIP
Glycated peptide

ABSTRACT

Molecularly imprinted polymer (MIP) nanofilms have been successfully implemented for the recognition of different target molecules: however, the underlying mechanistic details remained vague. This paper provides new insights in the preparation and binding mechanism of electrosynthesized peptide-imprinted polymer nanofilms for selective recognition of the terminal pentapeptides of the ß-chains of human adult hemoglobin, HbA, and its glycated form HbA1c. To differentiate between peptides differing solely in a glucose adduct MIP nanofilms were prepared by a two-step hierarchical electrosynthesis that involves first the chemisorption of a cysteinyl derivative of the pentapeptide followed by electropolymerization of scopoletin. This approach was compared with a random single-step electrosynthesis using scopoletin/pentapeptide mixtures. Electrochemical monitoring of the peptide binding to the MIP nanofilms by means of redox probe gating revealed a superior affinity of the hierarchical approach with a K_d value of 64.6 nM towards the related target. Changes in the electrosynthesized non-imprinted polymer and MIP nanofilms during chemical, electrochemical template removal and rebinding were substantiated *in situ* by monitoring the characteristic bands of both target peptides and polymer with surface enhanced infrared absorption spectroscopy. This rational approach led to MIPs with excellent selectivity and provided key mechanistic insights with respect to electrosynthesis, rebinding and stability of the formed MIPs.

1. Introduction

Molecular imprinting is a universal concept to generate materials with "molecular memory" by polymerizing suitable functional monomers in the presence of a target molecule, which act as template [1–3]. The subsequent removal of the template is expected to create recognition sites in the molecularly imprinted polymer (MIP) that can, further on, selectively rebind the target. Beside their fully synthetic generation MIPs have two essential advantages in comparison with natural affinity reagents, such as antibodies: i) higher stability under harsh environmental conditions and ii) lower production costs. The versatility of MIP synthesis is especially apparent in case of biomacromolecular targets, where to circumvent permanent entrapment of the template, the characteristic dimensions of the MIPs have been reduced to the nanoscale by using nanofilms or particles, as well as surface-imprinting techniques [4–7]. These can be combined by using for imprinting only a small fragment of the target analyte as template, which provides additional benefits in terms of selectivity and cost-reduction. In case of peptide and protein targets, imprinting of a peptide template is the key step of epitope imprinting. This term was first proposed by Rachkov and Minoura [8] to emphasize the similarity to the immunological determinants recognized by an antibody [9–12]. Template fragments (epitopes) include peptides [13–27], carbohydrates and engineered tags [28–33], or chemical labels [32,34]. The resulting MIPs have been shown to recognize both the target fragment

* Corresponding authors.
E-mail addresses: giorgio.caserta@tu-berlin.de (G. Caserta), robertgy@mail.bme.hu (R.E. Gyurcsányi), ingo.zebger@tu-berlin.de (I. Zebger), fschell@uni-potsdam.de (F.W. Scheller).

https://doi.org/10.1016/j.electacta.2021.138236

and whole protein [9,11–13,15,21,22,35]. Whilst the initial concept involved a homogeneous mixture of peptide and monomer, Shea's group introduced a heterogeneous version by attaching the peptide on a solid carrier prior to the photochemical polymer formation with clear benefit in terms of creating more uniform cavities [15]. Another approach from Bülowś group [19] generated the template immobilizing hemoglobin (HbA) via its accessible terminal peptides (including the N-terminal valines) to silica nanoparticles, followed by trypsin-mediated protein digestion. The methylacrylic acid-based MIPs showed a two-fold higher HbA binding as compared with the non-imprinted polymer (NIP), along with a discrimination of myoglobin and bovine serum albumin (BSA).

Electrochemical polymerization, an inherently surface-confined process, offers better means to control the polymer film growth. Therefore, we introduced fully electrosynthesized peptide imprinted nanofilms by growing the polymeric structure around an immobilized peptide [13].

Following this concept, this paper provides new insights in the preparation and binding mechanism of electrosynthesised peptide-imprinted polymer nanofilms for selective recognition of the terminal pentapeptides of the ß-chains of human adult hemoglobin (HbA) and its glycated derivative (HbA1c), which are the targets of the IFCC (International Federation of Clinical Chemistry) reference method for HbA1c.

Previous studies have reported the selective recognition of glycated peptides and glycoproteins by MIPs, mostly assisted by boronate affinity [31,32,36–38] that takes advantage of the inherent affinity of boronic acids toward diols. The boronic acid anchors were either bound to an underlying surface [38] or implemented in the polymer network [31]. Binding of artificially glycosylated peptides to the boronate-functionalized SAMs (self-assembled monolayers) resulted in uniform binding cavities [25]. This approach has been applied for the C-terminal nonapeptides from human ß2-microglobulin and myoglobin. Thus, while the molecular imprinting concept is universal, the monomer library used for MIP preparation in many cases takes advantage of "target-specific" monomers to increase the affinity of the respective MIPs. Consequently, the development of MIPs would be substantially facilitated if generic monomers could be used for the synthesis of similarly affine and selective polymers, recognizing different targets through a genuine molecular imprinting process. Therefore, in this study we have chosen a generic monomer devoid of boronate functionalization, namely scopoletin, in order to prepare MIP nanofilms capable to differentiate between peptides varying solely in a glucose adduct. Scopoletin forms by electropolymerization a conformal, insulating polymeric nanofilm on the electrode surface. Its generic use is supported by application to form MIPs for selective recognition of both low-molecular weight targets [13] and proteins [39–43], and its compatibility with a wide range of template removal procedures including chemical [39,44], electrochemical [13,21], and enzymatic processes [43].

Here, a two-step hierarchical electrosynthesis was chosen involving firstly the chemisorption of a cysteinyl derivative of the pentapeptide followed by electropolymerization of the scopoletin monomer. This approach was referenced to MIP nanofilms prepared by a random, single-step electrosynthesis of scopoletin/pentapeptides mixtures. Using *in situ* surface enhanced infrared absorption spectroscopy (SEIRAS), we detected structural changes in electrosynthesized non-imprinted polymers (NIPs) and MIPs during chemical as well as electrochemical template removal and rebinding by monitoring the characteristic marker bands of both target peptides and polymer. Peptide (re)binding to the MIP nanofilms was quantified via redox probe gating, allowing us to compare the selectivity for glycated and non-glycated peptides relevant for the quantification of HbA and HbA1c protein samples.

2. Experimental

2.1. Chemicals and reagents

Scopoletin (7-hydroxy-6-methoxycoumarin) was purchased from Sigma Aldrich (Steinheim, Germany). Potassium hexacyanoferrate (III) and potassium hydroxide from Roth (Karlsruhe, Germany); potassium dihydrogen phosphate, potassium hexacyanoferrate (II) trihydrate were obtained from Merck (Darmstadt, Germany); disodium phosphate from Duchefa Biochemie (Haarlem, the Netherlands); the peptides: the cysteine-extended N-terminus of ß-chain of HbA (CVHLTP-amide) herein referred as cys-peptide or CVHLTP, the N-terminus of ß-chain of HbA (VHLTP-amide) herein referred as N-terminal peptide or VHLTP, the peptide in which histidine was replaced by alanine (VALTP-amide) herein referred as VALTP, the glycated peptide with fructosyl valine at its terminus (Fruc-VHLTP-amide) herein referred as Fruc-peptide or Fruc-VHLTP and the C-terminal peptide of BSA (VVSTQ-amide) were purchased from Biosyntan GmbH (Berlin, Germany). All solutions were prepared with deionized water (DI water) obtained from a water purification system Milli-Q from Merck Chemicals GmbH (Darmstadt, Germany).

2.2. Electrochemical measurements

Square wave voltammetry (SWV) was carried out in 1 mL solution of 5 mM ferri/ferrocyanide in phosphate buffered saline, pH 7.4 (PBS) containing 10 mM KCl with a CHI 440 electrochemical workstation (CH Instruments Inc., Austin, USA) using a one-compartment three-electrode electrochemical cell. Gold wires (diameter of 0.5 mm from Goodfellow, Germany) were used as working electrodes, a spiral platinum wire as the counter electrode and Ag/AgCl as reference electrode (RE-3V from ALS Co., Japan). The potential was scanned from -0.3 to +0.4 V at a frequency of 10 Hz, an amplitude of 50 mV and a step height of 3 mV. All measurements were carried out at room temperature.

2.3. MIP-electrosynthesis, template removal and rebinding

The gold wire electrodes were cleaned in boiling 2.5 M KOH for 4 h followed by storage in concentrated H_2SO_4 overnight. Before usage, the electrodes were rinsed with deionized (DI) water and kept in 65% HNO_3 for 10 min. After rinsing with DI water again, the electrodes were ready for use. For the two-step hierarchical imprinting process via a chemisorbed "pre-immobilized" peptide, the clean bare gold wire electrodes were firstly incubated for 5 min in a PBS solution containing 50 μM cys-peptide at room temperature resulting in a sub-monolayer coverage of the electrode. The polyscopoletin layer was then deposited around the chemisorbed cys-peptide by electropolymerizing a solution containing 0.5 mM scopoletin, 10 mM NaCl and 5% V/V ethanol with 30 repetitive pulse cycles each comprising of a 0.0 and +0.7 V pulse for 5 and 1 s, respectively. Non-imprinted polymers were prepared using the same workflow lacking the initial cys-peptide chemisorption. After synthesis of the polymer layer, the electrodes were carefully rinsed with DI water and then dried gently under a nitrogen stream. To remove the immobilized cys-peptide, anodic oxidation of the thiol-gold bonds was performed by applying a potential of +900 mV on the MIP-electrode for 30 s in PBS. After template removal, the MIP-electrode was rinsed with DI water for several times and dried with nitrogen stream gently.

The monomer/peptide mixture-based MIPs (random MIPs) were synthesized on clean bare gold wire electrodes from a solution containing 0.5 mM scopoletin and 50 μM of either N-terminal peptide or Fruc-peptide, by applying the same pulse cycles as for hierarchical-MIP. Template removal was accomplished as described for the hierarchical-MIP.

For rebinding experiments, the electrode was placed in 1 mL PBS solution of 5 mM ferri/ferrocyanide containing 10 mM KCl in the stirred measuring cell followed by sequential addition of 2 μL of the peptide stock solution. To follow the kinetics of rebinding, SWV measurements were performed every 2 min without stirring the solution and the procedure was repeated until a steady state was reached.

2.4. SEIRA spectroscopic measurements

NIP and MIP films were also prepared on nanostructured gold electrodes suitable for SEIRA spectroelectrochemical investigations. This *in situ* technique allows the acquisition of IR spectra of each step of the polymer synthesis. Since the surface enhancement factor decays with increasing distance d with $1/d^6$ from the gold surface, this method is ideal for monitoring events in very close proximity to the gold surface (about 8 nm) [45]. A gold film was chemically deposited on a silicon prism for ATR (attenuated total reflection) studies and subsequently electrochemically cleaned to reveal an island-like nanostructure as described by Miyake *et al.* [46]. The prism was then installed into a home-made spectroelectrochemical IR cell, which was mounted in an IFS66v/S FTIR spectrometer from Bruker equipped with a liquid nitrogen cooled MCT (Mercury-Cadmium-Telluride) detector. The gold film served as working electrode, whereby a Pt wire and an Ag/AgCl electrode were used as counter and reference electrodes, respectively. Spectra with 4 cm^{-1} resolution were recorded by averaging 400 scans. For binding tests, the peptides were dissolved in deionized water (5 mM stock solution) and then diluted in PBS to a final concentration of 50 µM. Infrared spectra were registered during and after peptide immobilization. A further spectrum was recorded after extensive rinsing with buffer, which confirmed a stable binding of the target peptides. The buffer was then replaced by a scopoletin solution (0.5 mM, 10 mM NaCl, 5% V/V ethanol) and electrochemical synthesis of the MIP was carried by applying 30 pulse cycles starting with 0.0 V for 5 s and 0.7 V for 1 s. Non-imprinted polymers were prepared with the same workflow just without the target peptides. Template was removed from the gold surface by holding a potential of +900 mV (vs Ag/AgCl) for 30 s and monitoring the spectral changes. Rebinding was also verified by means of SEIRA spectroscopy.

2.5. Atomic force microscopic investigations

AFM measurements were carried out with Nanosurf FlexAFM (Switzerland) using Tap190Al-G cantilever (BudgetSensors, force constant: 48 N/m, length: 225 μm, tip radius $<$ 10 nm). The thickness of the polymer film was determined after electropolymerization at three places, according to the following steps. First, a 3 $\times$ 3 μm area was scanned in Tapping mode (resolution: 300 points/line, set point: 88–91%, free amplitude: 400 mV) to obtain topographic image of the film. Subsequently, the polymer was removed in 3 consecutive cycles on a 1 $\times$ 1 μm area in Lateral Force mode applying 1 μN force (resolution: 200 points/line). Finally, a 3 $\times$ 3 μm area was scanned to include the polymer-stripped region in Tapping mode with the same parameters. The obtained images were analyzed with Gwyddion software. The film thickness was determined as the average difference between the polymer height and the liberated gold surface.

3. Results and discussion

3.1. Interaction of peptide templates with bare gold electrodes

We considered the template (and control) peptide adsorption onto the gold surface for both types of MIP synthesis (Scheme 1), i.e. (i) the random single-step synthesis by electropolymerizing mixtures of scopoletin and the (cys-fee) N-terminal pentapeptide VHLTP as well as (ii) the two-step hierarchical approach involving first the chemisorption of the CVHLTP peptide via the thiol group of the terminal cysteine followed by electropolymerization.

In the first case a spontaneous adsorption of the (cys-free) VHLTP from the mixture with scopoletin is expected prior the electropolymerization. The peptide presence on the surface of the gold electrode was monitored by evaluating the suppression of the SWV signal of the redox marker ferri/ferrocyanide and the appearance of the characteristic amide I and amide II bands of the adsorbed peptides in the SEIRA spectra (Fig. S1, Appendix A. Supplementary data). The electrode incubation in both CVHLTP peptide and (cys-free) VHLTP solutions induced a concentration dependent decrease of the ferri/ferrocyanide signal on the gold electrodes, approaching saturation above 0.6 μM. The signal suppression at the saturation level was around two-fold higher for the cys-extended peptide than for the cys-free target obviously related to a stronger interaction with the electrode surface due to the formation of the Au-S bond (Fig. S1A). In case of the VALTP peptide, where the histidine is substituted by alanine, a weaker adsorption is found, suggesting that histidine also plays a role within the binding interaction to bare gold [47]. This was also verified by SEIRA spectroscopic experiments, in which it could be shown that CVHLTP and VHLTP peptides were indeed stably bound to the gold surface, while the VALTP peptide could be removed using a 0.8 M NaCl solution. CVHLTP and VHLTP, on the contrary, could be removed only by anodic polarization at +900 mV vs. Ag/AgCl (Fig. S1B).

3.2. Characterization of the NIP by SWV and SEIRA spectroscopy

The formation of the NIP-film by electropolymerization of scopoletin led to an almost complete suppression of the SWV signal of ferri/ferrocyanide and the appearance of characteristic polymer marker bands in the SEIRA spectrum (Fig. 1A). Two dominant bands, namely the C=O stretching vibration at 1715 cm^{-1} and the C–O stretching vibration at ca 1280 cm^{-1} suggest that the lactone ring is incorporated in the polymer structure. The bands in the range of 1600–1400 cm^{-1} are related preferentially to the aromatic C=C ring stretching vibrations, confirming that the coumarin unit remains intact. Additionally, the spectrum of the scopoletin monomer exhibits a strong IR absorption band at ca 1235 cm^{-1} (Fig. 1a, bottom trace), which can be attributed to the C–O stretching of the phenolic hydroxyl group. The time course of this band allows us to suggest a polymerization mechanism (Fig. S2). Its disappearance in the spectrum of the newly formed polymer (Fig. 1a, top trace) could be explained by the oxidation of the OH group in the monomer function. This mechanism is further supported by the spectral appearance of an intense band at 1160 cm^{-1} attributable to the C–O–C stretching of alkyl ethers, which is absent in the corresponding monomer spectrum. Therefore, the presumed polyscopoletin structure comprises a poly(alkyl ether) with a poly(ethylene oxide) backbone and coumarin side groups, in line with previous reports on the oxidative spectroelectrochemistry of coumarins (Fig. S2) [48]. The poly(ethylene oxide) backbone represents the hydrophilic part interacting with H_2O molecules, offering the possibility of H-bonding interactions with target molecules. The coumarin side groups, on the contrary, allow noncovalent π-π and hydrophobic interactions with the analyte. The application of an anodic potential of +900 mV did not influence the intensity of

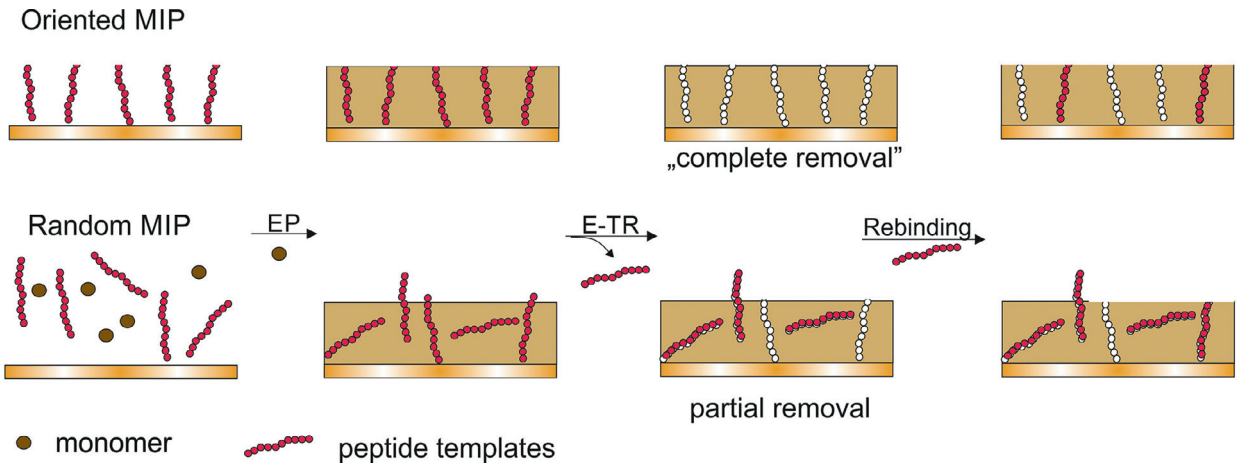

Scheme 1. Schematics of the hierarchical (oriented) MIP and random MIP preparations by electropolymerization (EP), electrochemical template removal (E-TR) and template rebinding. In case of hierarchical approach a chemisorbed peptide is anchored to the gold surface using the cysteine labeled VHLTP peptide, followed in a second step by controlled EP of scopoletin. The random MIP preparation comprises EP of the scopoletin / peptide mixtures. Considering that the E-TR process is largely constricted to peptides in contact with the underlying gold electrode, the oriented approach should grant a higher density and more homogenous orientation of the template during polymerization.

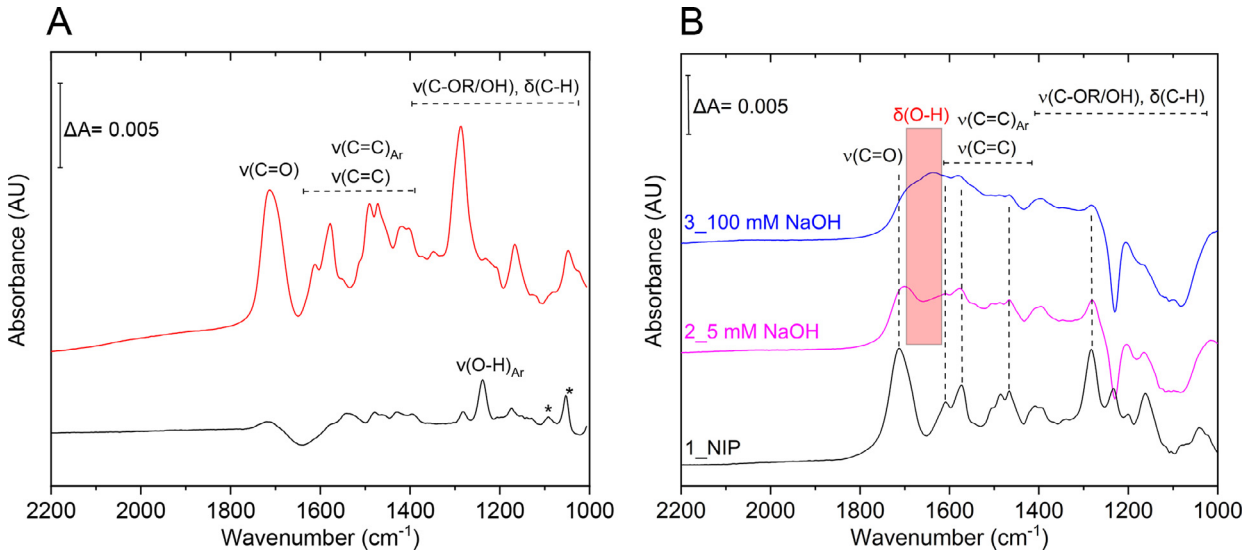

Fig. 1. IR spectroscopic characterization of the polyscopoletin films (NIP) on a SEIRA active gold electrode. (A) Absorbance spectra of the formed NIP-film after electropolymerization (EP) [red] and the scopoletin monomer before EP [black]. Observed modes are attributed to the carbonyl ν(C=O) stretching vibration (1715 cm^{-1}), aromatic and vinyl ν(C=C) stretching modes (1600–1400 cm^{-1}), ν(C–O) stretching vibration of the ester group (1280 cm^{-1}), the ν(C–O–C) stretching of alkyl ethers (1160 cm^{-1}) and δ(C–H) bending modes (1400–1000 cm^{-1}). Asterisks refer to spectral contribution of residual ethanol before EP. (B) Absorbance spectra displaying the NIP decomposition upon NaOH incubation. Trace 1 (black) shows characteristic polymer related vibrational modes before NaOH treatment; trace 2 (magenta) was recorded after short exposure (5 min) to a 5 mM NaOH solution followed by buffer exchange; trace 3 (blue) was recorded after short exposure (5 min) to 100 mM NaOH followed by buffer exchange. The described time interval is related to the sum of the acquisition time of a single spectrum in the presence of NaOH (~ 2 min), the subsequent washing step with PBS buffer and the acquisition of a second spectrum in PBS (about 2 min), which is required for calculating the resulting absorbance spectra. The ν(C=O) stretching vibration at 1715 cm^{-1} and several ν(C=C) strech related bands (black dashed lines) vanish with the concomitant appearance of δ(O–H) bending modes at about 1640 cm^{-1}, related to surface bound water molecules (red rectangle), indicating NIP decomposition.

the polyscopoletin related features in both SWV and SEIRA spectra indicating an intact polymer layer on the electrode surfaces. This result was confirmed by AFM measurements (Fig. 2) which revealed that the average thickness of the NIP-film after electropolymerization (9.3 ± 0.8 nm) did not change after anodic potential pulses of +900 mV (9.6 ± 0.1 nm).

On the other hand, application of an anodic potential of +950 mV resulted in a pronounced increase of the SWV peak indicating an increased permeability of the NIP-film. Furthermore, incubation of the NIP in 5 mM and 100 mM NaOH solutions, applied conditions used to remove the target from scopoletin-based MIPs [39,44], strongly affected the polymeric structure as derived from the disappearance of its characteristic marker band at 1715 cm^{-1} and the concomitant appearance of O–H bending vibrations at about 1640 cm^{-1} related to surface adsorbed water molecules (Fig. 1B). This points to an opening of the scopoletin lactone ring under alkaline conditions [49], thereby explaining the increased permeability of the NIP-film and the spectral detectability of water modes. These observations show that caution needs to be taken with respect to a manipulation of scopoletin-derived nanofilms, as it may lead to an erroneous interpretation of target (re)binding.

3.3. Characterization of the hierarchical- MIP nanofilm

Attempts to monitor the time course of CVHLTP peptide binding to the gold electrode evidenced that after 5 min ca 70% of the maximum absorption signals are detected, reaching saturation af-

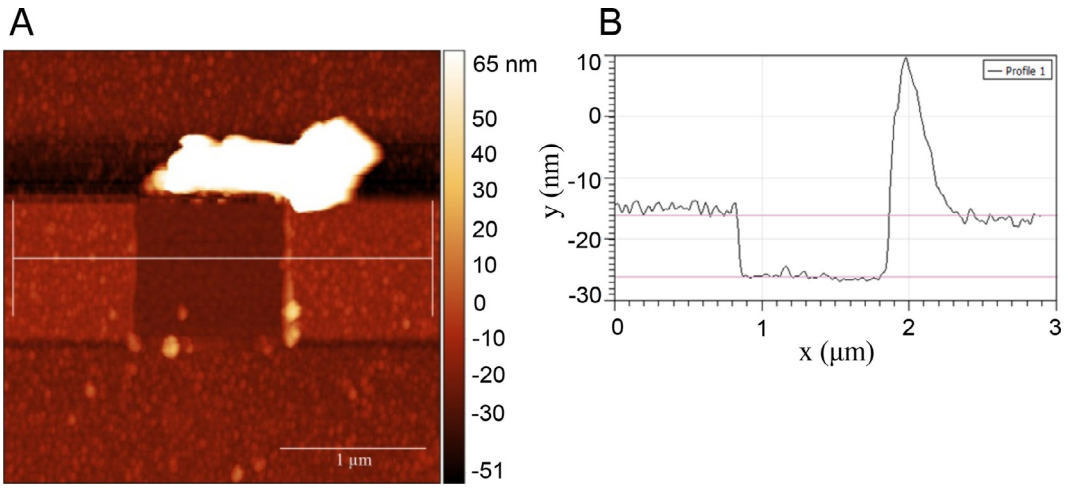

Fig. 2. (A) Topographic image of the non-imprinted polymer after removal of a 1 × 1 μm area. (B) The cross-section of the film used for thickness measurements.

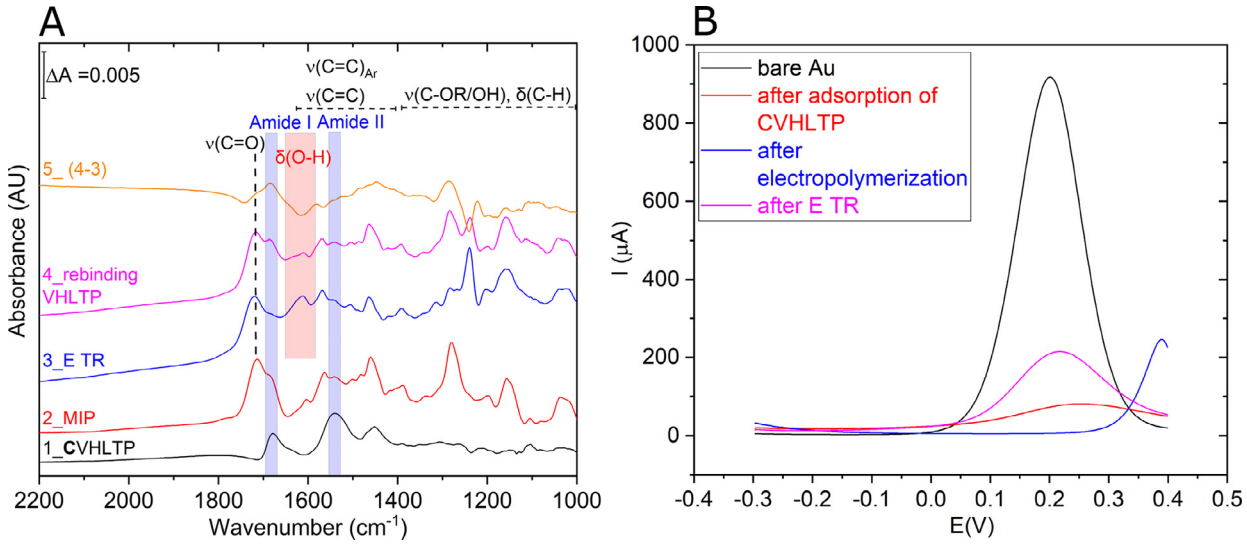

Fig. 3. (A) IR absorbance spectra of the individual steps of the SAM-MIP formation on a SEIRA active gold electrode. The observed vibrations related to the newly formed polymer are described in Fig. 1. The corresponding amide I and II bands at 1678 cm^{-1} and 1545 cm^{-1}, respectively, which are characteristic for the initially adsorbed cys-peptide (CVHLTP, trace 1) are marked with blue rectangles. Electrochemical template removal (trace 3, E-TR) is monitored through the appearance of a broad absorption band at ca. 1640 cm^{-1} attributed to the δ(O–H) bending vibrations (red rectangle) of surface-bound water molecules as consequence of the permeability of the MIP-film. After rebinding of VHLTP peptide (trace 4), the amide I band can be detected again, which can be derived more clearly from trace 5, i.e. the corresponding difference spectrum between trace 4 and trace 3. (B): SWV current responses of all steps of the SAM-MIP formation on a gold electrode before (black) and after adsorption of cys-peptide (red) followed by electropolymerization of scopoletin (blue) and electrochemical template removal (E-TR, pink).

ter ca 30 min (Fig. S3A). The short incubation time, resulting in a sub-monolayer covering the gold electrode (Fig. S3B), was applied for optimal MIP synthesis, while longer incubation times affected the subsequent polyscopoletin electrodeposition (Fig. S3C, *vide infra*). Scopoletin electropolymerization around the chemisorbed peptide target was monitored via the characteristic polymer bands in the SEIRA spectra (Fig. 3A, traces 1 and 2). Here, the presence of the cys-peptide in the polymer matrix was confirmed by the spectral detectability of the amide I band at 1678 cm^{-1} as shoulder of a dominant absorption band of the polymer, i.e., the C=O stretching vibration at 1715 cm^{-1} (Fig. 3A, trace 2). The first is absent in the IR spectrum of the NIP (Fig. 1A). MIP formation was also validated by the almost complete suppression of the ferri/ferrocyanide redox marker in the SWV experiments (Fig. 3B, blue trace).

Peptide removal from the MIP matrix was achieved by polarizing the electrode at +900 mV, which resulted in a drastic increase of the SWV signal of the redox marker and the spectral disappearance of the peptide characteristic amide I band (Fig. 3A and 3B).

Notably, the characteristic infrared signature of the polyscopoletin unit was not affected (Fig. 3A, black dashed line), confirming the stability of the polymer to the template removal conditions. The IR spectroscopic characterization of the entire MIP workflow revealed that the template removal from the gold surface is accompanied by spectral appearance of O–H stretching (3200–3500 cm^{-1}) and O–H bending (1600–1680 cm^{-1}, centered at 1640 cm^{-1}) vibrations from H_2O molecules that diffuse towards the gold electrode surface due to free cavities in the MIP film (Fig. 3A, red rectangle, trace 3). Rebinding experiments using cys-free peptide showed a re-appearance of the amide I band in the corresponding SEIRA spectrum (Fig. 3A, trace 4, blue rectangles). Indeed, the IR difference spectrum of "target rebinding" minus the "template removal" step (Fig. 3A, trace 5), exhibits a positive amide I band in combination with a negative band related to O–H bending vibrations deriving from surface released water molecules. Additional control experiments were performed incubating a NIP film with 50 µM VHLTP/VALTP peptides. Within this treatment no pep-

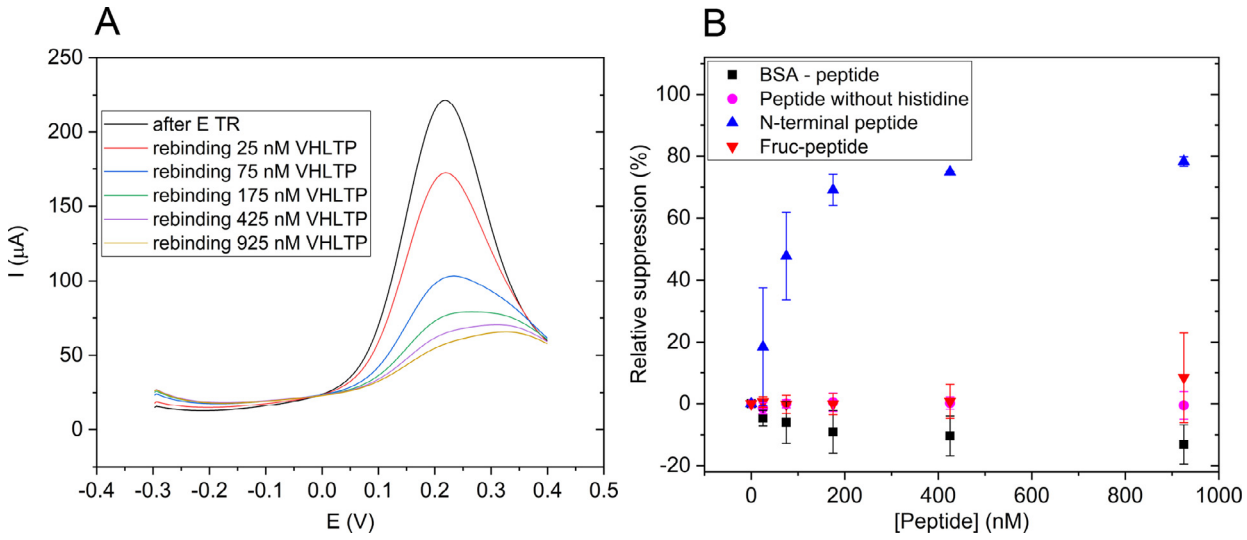

Fig 4. Concentration dependent SWV (A) responses of the rebinding of VHLTP (N-terminal peptide) and (B) the relative signals of the rebinding of VHLTP (blue) and related peptides to the hierarchical-MIP. Red: Fruc-VHLTP; magenta: VALTP (peptide without histidine); black: C-terminal peptide of BSA.

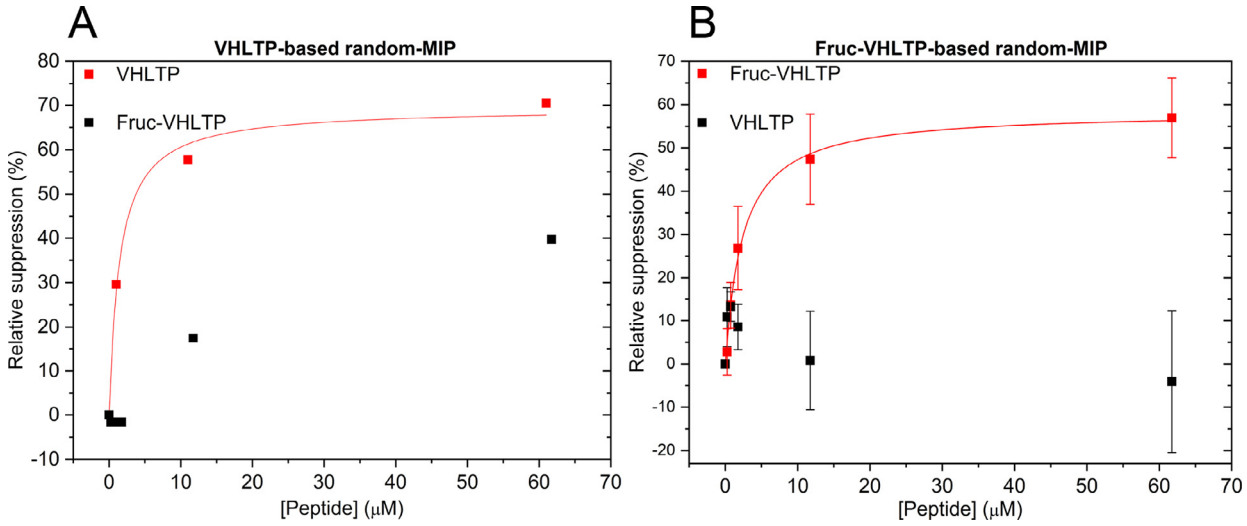

Fig. 5. Concentration dependent relative suppression of the SWV signal (peak current) produced by increasing concentrations of VHLTP and Fruc-VHLTP peptides using random MIPs imprinted with (A) VHLTP and (B) Fruc-VHLTP templates.

Table 1
Experimental K_d values for the binding of peptides to the different MIPs in this work.

MIP	Target	K_d
Hierarchical-MIP (VHLTP template)	VHLTP	64.6 ± 12.9 nM
Random-MIP (VHLTP template)	VHLTP	1.4 ± 0.3 μM
Random-MIP (Fruc-VHLTP template)	Fruc-VHLTP	2.4 ± 0.3 μM

tide characteristic amide I/II bands could be detected in the SEIRA spectra (Fig. S4).

The rebinding of VHLTP could be followed also through SWV. After injection of the peptide into the electrochemical cell, the SWV peak decreased and reached a steady state within 25 min (Fig. S5). This process could be monitored *in situ*, by recording the rebinding in the presence of the redox marker. The relative decrease of the peak current was linearly dependent on the peptide concentration up to 100 nM and reached saturation above 200 nM (Fig. 4), resulting in a K_d value of 64.6 nM (Table 1).

In order to characterize the cross-reactivity of the MIP-sensor, the interaction with further peptides, such as a Fruc-peptide (Fruc-VHLTP), the peptide without histidine (VALTP) and the C-terminal peptide of BSA was investigated. As displayed in Fig. 4B, the binding of the imprinted template was highly specific as compared with the other peptides. Substitution of a histidine residue by alanine or introduction of a fructosyl residue at the N-terminal valine decreased the saturation value by a factor of almost eight, revealing the sequence specificity of the MIP cavities. These values are comparable to the related data reported in literature for peptides with a single amino acid mismatch [13,15].

3.4. Characterization of the MIPs prepared from the peptide-monomer mixture

The random-MIP was synthesized from a solution of 50 μM VHLTP (the N-terminal peptide) and 0.5 mM scopoletin using the same pulse voltammetric procedure as in case of the SAM-based MIPs. After 30 s application of a potential of +900 mV for template removal, the SWV peak height was around 70 μA, which was 2–3 times lower than that of hierarchical-MIP (data not shown). In order to gain structural information of this particular synthesis approach, SEIRA spectroelectrochemistry was used to map the en-

tire workflow (Fig. S6). After the random-MIP was formed (Fig. S6, trace 2), the subsequent template removal by anodic polarization at +900 mV leads only to a partial detachment of target peptide (Fig. S6, trace 3). This is also confirmed by the observed minor rebinding compared to the experiment using the hierarchical approach (Fig. S6 and Fig. 2A). A plausible explanation of the differences observed between the hierarchical and random approaches arises from the non-homogenous peptide distribution (and their partial entrapment) within the polymer matrix using the latter method.

The rebinding of VHLTP peptide, within the random-MIP reached its saturation level at around 10 μM (Fig. 5A) with a K_d value of 1.4 μM by using the Langmuir isotherm model (Table 1). This suggests a significantly weaker interaction as compared to the hierarchical-MIP, which reached saturation already at ca. 200 nM (K_d = 64.6 nM, Table 1). Besides, while both types of MIPs showed preferential binding of the target peptide, the discrimination of the Fruc-VHLTP was less effective using the VHLTP imprinted sites of the random-MIP approach (Fig. 5A) as compared with their hierarchical-based analogues (Fig. 4B).

The results suggest a superiority in terms of binding affinity and selectivity of the hierarchical-MIPs, which is presumably related to the higher density and more homogenous orientation of the template during polymerization. The latter approach created more effective imprinted binding sites than the non-homogenously oriented peptides in the mixture method, as confirmed by infrared spectroscopic data (Fig. 3A and Fig. S6). The random-MIP imprinting approach was also applied for the Fruc-VHLTP target. Notably, in comparison with the corresponding results for the N-terminal (VHLTP) peptide target (Fig. 5A), the binding difference between the VHLTP and Fruc-VHLTP was more pronounced (Fig. 5B). A K_d value of 2.4 μM was determined for the binding of Fruc-VHLTP, whereas no measurable affinity for the VHLTP (without fructose) could be detected (Fig. 5B, Table 1).

4. Conclusions

In this work, MIPs for the recognition of the N-terminal peptide of human adult hemoglobin and its glycosylated variant (HbA1c) have been synthesized by electropolymerizing scopoletin either after chemisorption of the cys-extended peptide or just as mixture with the target. Surface enhanced infrared absorption spectroscopy has been successfully applied *in situ* monitoring (both) peptides and polymer specific vibrations. In this respect, we observed that the stepwise approach (hierarchical-MIP) ensures subtle control of the MIP workflow as outlined in Scheme 1.

Notably, multiple variables affect an “adequate” electrosynthesis of a MIP nanofilm. The first bottleneck is the incubation time of the target on the electrode. Short incubation times resulting in a sub-monolayer coverage, are highly desirable to achieve a proper polyscopoletin electrodeposition. Here, the hydrophilic poly(ethylene oxide) backbone offers the possibility of H-bonding interactions with target molecules while the aromatic coumarin side groups ensure noncovalent π-π and hydrophobic interactions with the analyte. Secondly, electrochemical template removal (E-TR) should be preferred to chemical procedures. Indeed, the polyscopoletin scaffold remains unaffected during the entire electrochemical workflow as corroborated by AFM measurements. On the contrary, chemical treatment with NaOH, which is often used to remove peptide/protein targets, results in the coumarin scaffold degradation. This, in turn, might lead to improper (re)binding, as the redox probe cannot distinguish between the imprinted cavities and the new “sites” originating from degradation.

In addition, we detected the binding of water molecules after the electrochemical driven cavity formation by SEIRAS. Their observed removal during peptide rebinding in the “oriented” approach provides, thus, new insights into so far vague mechanism of target rebinding.

Both MIPs exhibit binding specificity with respect to the target peptide and can discriminate single mismatches of the pentapeptide or the addition of fructose at the terminal valine. This was achieved using the generic scopoletin monomer lacking of specific functionalities with intrinsic selectivity for sugar residues, i.e. without taking advantage of boronate affinity. The hierarchical-based MIP displays a much higher affinity as reflected by the smaller K_d value of 64.6 nM compared to the random-MIP approach with a K_d of 1.4 μM (Table 1), indicating that homogenous orientation and accessibility of the binding cavities are important for the analytical performance. Given their practically specific response to the peptide templates, the respective MIPs show clear potential for the quantification of both the glycated and the non-glycated N-terminal peptides.

Declaration of Competing Interest

There are no conflicts to declare.

Credit authorship contribution statement

Giorgio Caserta: Investigation, Methodology, Formal analysis, Writing – original draft, Writing – review & editing. **Xiaorong Zhang:** Investigation, Methodology, Formal analysis, Visualization. **Aysu Yarman:** Methodology, Formal analysis, Supervision. **Eszter Supala:** Investigation, Formal analysis, Visualization. **Ulla Wollenberger:** Writing – review & editing, Funding acquisition. **Róbert E. Gyurcsányi:** Methodology, Formal analysis, Visualization, Writing – original draft, Writing – review & editing, Funding acquisition. **Ingo Zebger:** Methodology, Formal analysis, Writing – review & editing, Funding acquisition. **Frieder W. Scheller:** Conceptualization, Supervision, Writing – original draft, Writing – review & editing, Project administration, Funding acquisition.

Acknowledgements

F.W.S., I.Z., U.W., and A.Y. acknowledge the Deutsche Forschungsgemeinschaft (DFG, German Research Foundation) under Germanyś Excellence Strategy – EXC 2008 – 390540038 – UniSysCat for funding. Further, G.C. and I.Z. are grateful to the Einstein Foundation Berlin (grant number EVF-2016-277) for additional funding. The research of E.S. and R.Gy. has been supported by the NRDI Fund (TKP2020 IES, Grant No. BME-IE-NAT) based on the charter of bolster issued by the NRDI Office under the auspices of the Ministry for Innovation and Technology.

Supplementary materials

Supplementary material associated with this article can be found, in the online version, at doi:10.1016/j.electacta.2021.138236.

References

[1] R. Arshady, K. Mosbach, Synthesis of substrate-selective polymers by host-guest polymerization, Makromol. Chem. 182 (1981) 687–692, doi:10.1002/macp.1981.021820240.
[2] M. Hussain, J. Wackerlig, P. Lieberzeit, Biomimetic strategies for sensing biological species, Biosensors 3 (2013) 89–107, doi:10.3390/bios3010089.
[3] G. Wulff, A. Sarhan, Über die Anwendung von enzymanalog gebauten Polymeren zur Racemattrennung, Angew. Chem. 84 (1972) 364 364, doi:10.1002/ange.19720840838.
[4] J. Bognár, J. Szűcs, Z. Dorkó, V. Horváth, R.E. Gyurcsányi, Nanosphere lithography as a versatile method to generate surface-imprinted polymer films for selective protein recognition, Adv. Funct. Mater. (2013) n/a-n/a, doi:10.1002/adfm.201300113.
[5] A. Menaker, V. Syritski, J. Reut, A. Öpik, V. Horváth, R.E. Gyurcsányi, Electrosynthesized surface-imprinted conducting polymer microrods for selective protein recognition, Adv. Mater. 21 (2009) 2271–2275, doi:10.1002/adma.200803597.

[6] G. Ceolin, Á. Orbán, V. Kocsis, R.E. Gyurcsányi, I. Kézsmárki, V. Horváth, Electrochemical template synthesis of protein-imprinted magnetic polymer microrods, J. Mater. Sci. 48 (2013) 5209–5218, doi:10.1007/s10853-013-7309-6.
[7] J. Xu, E. Prost, K. Haupt, B. Tse Sum Bui, Direct and sensitive determination of trypsin in human urine using a water-soluble signaling fluorescent molecularly imprinted polymer nanoprobe, Sens. Actuators B Chem. 258 (2018) 10–17, doi:10.1016/j.snb.2017.11.077.
[8] A. Rachkov, N. Minoura, Towards molecularly imprinted polymers selective to peptides and proteins. The epitope approach, Biochim. Biophys. Acta BBA - Protein Struct. Mol. Enzymol. 1544 (2001) 255–266, doi:10.1016/S0167-4838(00)00226-0.
[9] K. Yang, S. Li, L. Liu, Y. Chen, W. Zhou, J. Pei, Z. Liang, L. Zhang, Y. Zhang, Epitope imprinting technology: progress, applications, and perspectives toward artificial antibodies, Adv. Mater. 31 (2019) 1902048, doi:10.1002/adma.201902048.
[10] M. Singh, N. Gupta, R. Raghuwanshi, Epitope imprinting approach to monitor diseases, J. Mol. Genet. Med. (2017) 11, doi:10.4172/1747-0862.1000270.
[11] J. Xu, H. Miao, J. Wang, G. Pan, Molecularly imprinted synthetic antibodies: from chemical design to biomedical applications, Small 16 (2020) 1906644, doi:10.1002/smll.201906644.
[12] B. Fresco-Cala, B. Mizaikoff, Surrogate imprinting strategies: molecular imprints via fragments and dummies, ACS Appl. Polym. Mater. 2 (2020) 3714–3741, doi:10.1021/acsapm.0c00555.
[13] D. Dechtrirat, K.J. Jetzschmann, W.F.M. Stöcklein, F.W. Scheller, N. Gajovic-Eichelmann, Protein rebinding to a surface-confined imprint, Adv. Funct. Mater. 22 (2012) 5231–5237, doi:10.1002/adfm.201201328.
[14] D.-Y. Li, X.-M. Zhang, Y.-J. Yan, X.-W. He, W.-Y. Li, Y.-K. Zhang, Thermo-sensitive imprinted polymer embedded carbon dots using epitope approach, Biosens. Bioelectron. 79 (2016) 187–192, doi:10.1016/j.bios.2015.12.016.
[15] H. Nishino, C.-S. Huang, K.J. Shea, Selective protein capture by epitope imprinting, Angew. Chem. Int. Ed. 45 (2006) 2392–2396, doi:10.1002/anie.200503760.
[16] Y.-P. Qin, C. Jia, X.-W. He, W.-Y. Li, Y.-K. Zhang, Thermosensitive metal chelation dual-template epitope imprinting polymer using distillation–precipitation polymerization for simultaneous recognition of human serum albumin and transferrin, ACS Appl. Mater. Interfaces. 10 (2018) 9060–9068, doi:10.1021/acsami.8b00327.
[17] K. Yang, S. Li, J. Liu, L. Liu, L. Zhang, Y. Zhang, Multiepitope templates imprinted particles for the simultaneous capture of various target proteins, Anal. Chem. 88 (2016) 5621–5625, doi:10.1021/acs.analchem.6b01247.
[18] C.-J. Zhao, X.-H. Ma, J.-P. Li, An insulin molecularly imprinted electrochemical sensor based on epitope imprinting,, Chin. J. Anal. Chem. 45 (2017) 1360–1366, doi:10.1016/S1872-2040(17)61039-9.
[19] H. Bagán, T. Zhou, N.L. Eriksson, L. Bülow, L. Ye, Synthesis and characterization of epitope-imprinted polymers for purification of human hemoglobin, RSC Adv 7 (2017) 41705–41712, doi:10.1039/C7RA07674F.
[20] K. Yang, J. Liu, S. Li, Q. Li, Q. Wu, Y. Zhou, Q. Zhao, N. Deng, Z. Liang, L. Zhang, Y. Zhang, Epitope imprinted polyethersulfone beads by self-assembly for target protein capture from the plasma proteome, Chem. Commun. 50 (2014) 9521–9524, doi:10.1039/C4CC03428G.
[21] Z. Altintas, A. Takiden, T. Utesch, M.A. Mroginski, B. Schmid, F.W. Scheller, R.D. Süssmuth, Integrated approaches toward high-affinity artificial protein binders obtained via computationally simulated epitopes for protein recognition, Adv. Funct. Mater. 29 (2019) 1807332, doi:10.1002/adfm.201807332.
[22] E. Moczko, A. Guerreiro, C. Cáceres, E. Piletska, B. Sellergren, S.A. Piletsky, Epitope approach in molecular imprinting of antibodies, J. Chromatogr. B. 1124 (2019) 1–6, doi:10.1016/j.jchromb.2019.05.024.
[23] P.S. Sharma, Z. Iskierko, K. Noworyta, M. Cieplak, P. Borowicz, W. Lisowski, F. D'Souza, W. Kutner, Synthesis and application of a "plastic antibody" in electrochemical microfluidic platform for oxytocin determination, Biosens. Bioelectron. 100 (2018) 251–258, doi:10.1016/j.bios.2017.09.009.
[24] X.-T. Ma, X.-W. He, W.-Y. Li, Y.-K. Zhang, Oriented surface epitope imprinted polymer-based quartz crystal microbalance sensor for cytochrome c, Talanta 191 (2019) 222–228, doi:10.1016/j.talanta.2018.08.079.
[25] R. Xing, Y. Ma, Y. Wang, Y. Wen, Z. Liu, Specific recognition of proteins and peptides *via* controllable oriented surface imprinting of boronate affinity-anchored epitopes, Chem. Sci. 10 (2019) 1831–1835, doi:10.1039/C8SC04169E.
[26] S.L. Moura, L.M. Fajardo, L. dos A. Cunha, M.D.P.T. Sotomayor, F.B.C. Machado, L.F.A. Ferrão, M.I. Pividori, Theoretical and experimental study for the biomimetic recognition of levothyroxine hormone on magnetic molecularly imprinted polymer, Biosens. Bioelectron. 107 (2018) 203–210, doi:10.1016/j.bios.2018.01.028.
[27] M.-H. Lee, K.-T. Liu, J.L. Thomas, Z.-L. Su, D. O'Hare, T. van Wuellen, J.M. Chamarro, S. Bolognin, S.-C. Luo, J.C. Schwamborn, H.-Y. Lin, Peptide-imprinted poly(hydroxymethyl 3,4-ethylenedioxythiophene) nanotubes for detection of α synuclein in human brain organoids, ACS Appl. Nano Mater. 3 (2020) 8027–8036, doi:10.1021/acsanm.0c01476.
[28] S. Li, K. Yang, J. Liu, B. Jiang, L. Zhang, Y. Zhang, Surface-imprinted nanoparticles prepared with a his-tag-anchored epitope as the template, Anal. Chem. 87 (2015) 4617–4620, doi:10.1021/ac5047246.
[29] S. Li, K. Yang, N. Deng, Y. Min, L. Liu, L. Zhang, Y. Zhang, Thermoresponsive epitope surface-imprinted nanoparticles for specific capture and release of target protein from human plasma, ACS Appl. Mater. Interfaces. 8 (2016) 5747–5751, doi:10.1021/acsami.5b11415.
[30] S. Li, K. Yang, B. Zhao, X. Li, L. Liu, Y. Chen, L. Zhang, Y. Zhang, Epitope imprinting enhanced IMAC (EI-IMAC) for highly selective purification of His-tagged protein, J. Mater. Chem. B. 4 (2016) 1960–1967, doi:10.1039/C5TB02505B.
[31] X. Ma, M. Li, P. Tong, C. Zhao, J. Li, G. Xu, A strategy for construction of highly sensitive glycosyl imprinted electrochemical sensor based on sandwich-like multiple signal enhancement and determination of neural cell adhesion molecule, Biosens. Bioelectron. 156 (2020) 112150, doi:10.1016/j.bios.2020.112150.
[32] J. Li, X. Ma, M. Li, Y. Zhang, Does polysaccharide is an idea template selection for glycosyl imprinting? Biosens. Bioelectron. 99 (2018) 438–442, doi:10.1016/j.bios.2017.08.004.
[33] X. Tu, P. Muhammad, J. Liu, Y. Ma, S. Wang, D. Yin, Z. Liu, Molecularly imprinted polymer-based plasmonic immunosandwich assay for fast and ultrasensitive determination of trace glycoproteins in complex samples, Anal. Chem. 88 (2016) 12363–12370, doi:10.1021/acs.analchem.6b03597.
[34] M. You, S. Yang, W. Tang, F. Zhang, P. He, Molecularly imprinted polymers-based electrochemical DNA biosensor for the determination of BRCA-1 amplified by SiO2@Ag, Biosens. Bioelectron. 112 (2018) 72–78, doi:10.1016/j.bios.2018.04.038.
[35] D.-F. Tai, C.-Y. Lin, T.-Z. Wu, L.-K. Chen, Recognition of dengue virus protein using epitope-mediated molecularly imprinted film, Anal. Chem. 77 (2005) 5140–5143, doi:10.1021/ac0504060.
[36] L. Li, Y. Lu, Z. Bie, H.-Y. Chen, Z. Liu, Photolithographic boronate affinity molecular imprinting: a general and facile approach for glycoprotein imprinting, Angew. Chem. Int. Ed. 52 (2013) 7451–7454, doi:10.1002/anie.201207950.
[37] R. Xing, S. Wang, Z. Bie, H. He, Z. Liu, Preparation of molecularly imprinted polymers specific to glycoproteins, glycans and monosaccharides via boronate affinity controllable–oriented surface imprinting, Nat. Protoc. 12 (2017) 964–987, doi:10.1038/nprot.2017.015.
[38] L. Zhou, Y. Wang, R. Xing, J. Chen, J. Liu, W. Li, Z. Liu, Orthogonal dual molecularly imprinted polymer-based plasmonic immunosandwich assay: a double characteristic recognition strategy for specific detection of glycoproteins, Biosens. Bioelectron. 145 (2019) 111729, doi:10.1016/j.bios.2019.111729.
[39] M. Bosserdt, J. Erdőssy, G. Lautner, J. Witt, K. Köhler, N. Gajovic-Eichelmann, A. Yarman, G. Wittstock, F.W. Scheller, R.E. Gyurcsányi, Microelectrospotting as a new method for electrosynthesis of surface-imprinted polymer microarrays for protein recognition, Biosens. Bioelectron. 73 (2015) 123–129, doi:10.1016/j.bios.2015.05.049.
[40] Z. Stojanovic, J. Erdőssy, K. Keltai, F.W. Scheller, R.E. Gyurcsányi, Electrosynthesized molecularly imprinted polyscopoletin nanofilms for human serum albumin detection, Anal. Chim. Acta. 977 (2017) 1–9, doi:10.1016/j.aca.2017.04.043.
[41] A. Yarman, Development of a molecularly imprinted polymer-based electrochemical sensor for tyrosinase, Turk. J. Chem. (2018) 42, doi:10.3906/kim-1708-68.
[42] A. Yarman, Electrosynthesized molecularly imprinted polymer for laccase using the inactivated enzyme as the target: electrosynthesized mip for laccase using the inactivated enzyme as the target, Bull. Korean Chem. Soc. 39 (2018) 483–488, doi:10.1002/bkcs.11413.
[43] X. Zhang, A. Yarman, J. Erdossy, S. Katz, I. Zebger, K.J. Jetzschmann, Z. Altintas, U. Wollenberger, R.E. Gyurcsányi, F.W. Scheller, Electrosynthesized MIPs for transferrin: Plastibodies or nano-filters? Biosens. Bioelectron. 105 (2018) 29–35, doi:10.1016/j.bios.2018.01.011.
[44] R. Tchinda, A. Tutsch, B. Schmid, R.D. Süssmuth, Z. Altintas, Recognition of protein biomarkers using epitope-mediated molecularly imprinted films: Histidine or cysteine modified epitopes? Biosens. Bioelectron. 123 (2019) 260–268, doi:10.1016/j.bios.2018.09.010.
[45] in: M. Osawa, Surface-enhanced infrared absorption, in: S. Kawata (Ed.), Field Opt. Surf. Plasmon Polaritons, Springer, Berlin Heidelberg, Berlin, Heidelberg, 2001, pp. 163–187, doi:10.1007/3-540-44552-8_9.
[46] H. Miyake, S. Ye, M. Osawa, Electroless deposition of gold thin films on silicon for surface-enhanced infrared spectroelectrochemistry, Electrochem. Commun. 4 (2002) 973–977, doi:10.1016/S1388-2481(02)00510-6.
[47] J.M. Kogot, H.J. England, G.F. Strouse, T.M. Logan, Single peptide assembly onto a 1.5 nm au surface via a histidine tag, J. Am. Chem. Soc. 130 (2008) 16156–16157, doi:10.1021/ja8064717.
[48] X.-R. Hu, J.-B. He, Y. Wang, Y.-W. Zhu, J.-J. Tian, Oxidative spectroelectrochemistry of two representative coumarins, Electrochimica Acta 56 (2011) 2919–2925, doi:10.1016/j.electacta.2010.12.086.
[49] R. Gómez-Bombarelli, E. Calle, J. Casado, Mechanisms of lactone hydrolysis in neutral and alkaline conditions, J. Org. Chem. 78 (2013) 6868–6879, doi:10.1021/jo400258w.